Polymer 50 (2009) 161–170

Contents lists available at ScienceDirect

Polymer

journal homepage: www.elsevier.com/locate/polymer

# The effect of the solvent on the morphology of cellulose acetate/montmorillonite nanocomposites

Rafaelle Bonzanini Romero, Carlos Alberto Paula Leite, Maria do Carmo Gonçalves*

*Institute of Chemistry, University of Campinas, P.O. Box 6154, 13083-970 Campinas, Sao Paulo, Brazil*

ARTICLE INFO

*Article history:*
Received 19 August 2008
Received in revised form
30 October 2008
Accepted 31 October 2008
Available online 17 November 2008

*Keywords:*
Cellulose acetate
Nanocomposites
Morphology

ABSTRACT

Nanocomposites of cellulose acetate and sodium montmorillonite were prepared using the solution intercalation method with different solvents. The effects of solvent type on the morphology, thermal and mechanical properties of the nanocomposites were investigated by X-ray microtomography and diffraction, field emission scanning electron microscopy, analytical transmission electron microscopy based on electron loss spectroscopy imaging and dynamical mechanical analysis. XRD and TEM results indicated that the dispersion and delamination of the clay are achieved when the solvent presents favorable interactions with the clay. In this case, the storage modulus and the glass transition temperature are significantly higher than those of pure cellulose acetate. The results show that the solvent has a major effect in controlling the morphology of cellulose acetate and cellulose acetate nanocomposite and could be used as a process parameter to produce films with a range of properties.



## 1. Introduction

Nanocomposites offer the potential for the diversification of applications of polymers due to their excellent properties such as high heat distortion temperature, dimensional stability, improved barrier properties, flame retardancy, and enhanced thermo-mechanical properties [1–5].

Biodegradable polymers from renewable resources are a fairly new area of nanocomposites which has attracted the attention of researchers with expertise in diverse areas [6–29]. Nanoreinforcement of bio-based polymers can be used to create new materials. Organic–inorganic materials are extraordinarily versatile as they could be formed from a large variety of biopolymers such as polysaccharides, polypeptides, proteins and nucleic acids, among others. Various nanoreinforcements are currently being developed, but the most intensively researched type of nanocomposite uses layered silicate clay mineral as the reinforcing phase due to its easy availability and low cost. Therefore, the development of biodegradable polymer-based nanocomposites can open the way towards innovative applications of polymers [5,7,11].

Renewable source-based biodegradable polymers, usually used for the preparation of nanocomposites, are polylactide (PLA) [2,15,16,30], poly(3-hydroxy butyrate) (PHB) [17] and its copolymers [18], thermoplastic starch [19,20], plant oils [21,22], cellulose [23–25], gelatine [26], chitosan [7,8,27–29].

Cellulose is the most abundant natural polymer on earth, which offers an attractive alternative to petroleum feedstocks when making plastics [23,31]. Cellulose biopolymers have recently been used in the preparation of nanocomposites as a potentially biodegradable polymer of natural origin. An approach to cellulose–clay systems has recently been reported by White [24] who described the development of cotton–clay nanocomposites with potential applications as a flame retardant.

Cellulose plastics such as cellulose acetate (CA), cellulose acetate propionate (CAP), cellulose acetate butyrate (CAB) and carboxymethyl cellulose acetate butyrate (CMCAB) are thermoplastic materials produced by the esterification of cellulose materials such as cotton, recycled paper, wood cellulose and sugarcane. These derivatives have been used for the applications in many areas such as laminates, optical films, textile fibers and coatings for pharmaceuticals and foods [32].

Cellulose acetate can also be considered as a good candidate for the preparation of biopolymer–clay nanocomposites owing to its potential biodegradability, excellent optical clarity and stiffness [7,25,32]. Cellulose acetate has already been used in diverse areas, such as filters, membranes, packing films, adhesives, coatings for paper and plastic products, electrical isolation and drug delivery systems [33,34]. Apart from this, nanocomposites based on cellulose acetate seem to be promising candidates for the development of plastic devices and more impermeable packing films and coatings.

Recently, Park et al. [13,14,23,25,35] have described the preparation of cellulose acetate with organoclay to form nanocomposites, by using triethyl citrate as a plastifier. The resulting materials

* Corresponding author. Tel.: +55 19 35213129; fax: +55 19 35213023.
*E-mail address:* maria@iqm.unicamp.br (M.doC. Gonçalves).

0032-3861/$ – see front matter © 2008 Elsevier Ltd. All rights reserved.
doi:10.1016/j.polymer.2008.10.059

exhibit interesting mechanical and vapour permeability behaviours that are associated with the nanostructural arrangement of the inorganic network in the polymeric matrix.

The interest in these materials is driven by the possibility of unusual physical property enhancements at low filler levels. The key to this performance lies in the ability to exfoliate and disperse individual, high-aspect ratio silicate platelets within the polymer matrix. An adequate choice of the intercalation method must be made in order to achieve the exfoliation and dispersion of clay particles. Polymer intercalation using the solution method is one of the processes that can be used for the preparation of nanocomposites. This method is based on a solvent system in which the polymer is soluble and the silicate layers are swellable. The solution method allows good control of the homogeneity of the constituents, and it helps to understand the intercalation process and the nanocomposite morphology [36,37].

In this work, cellulose acetate/sodium montmorillonite (CA/MMT) nanocomposites were prepared using the solution intercalation method with different solvents. The influence of solvent type on the nanocomposite structures, morphologies and thermal and mechanical properties was investigated by X-ray diffraction (XRD), X-ray microtomography, field emission scanning electron microscopy (FESEM), transmission electron microscope associated to electron loss spectroscopy (ESI-TEM) and dynamical mechanical analysis (DMA). The solution intercalation method was used to investigate the effect of the polymer–solvent, solvent–clay and polymer–clay interaction effects on the intercalation process.

## 2. Experimental

### 2.1. Materials

Cellulose acetate (CA) was purchased from Sigma–Aldrich, with 39.8 wt% acetyl content and 2.45 degrees of substitution. The number-average molar mass of the polymer ($M_n = 50\,000$ g/mol) was determined by gel permeation chromatography (GPC) using a Waters 510 series system and calibrated with polystyrene standards. A natural sodium montmorillonite (MMT) clay was used in this work. The Polenita clay, supplied by Eduardo Vasconcelos Representações LTDA (Porto Alegre, Brazil), is a polycationic clay with a cation exchange capacity of 62 mequiv/100 g and a real density of 2.47 g/cm$^3$. The elemental composition (wt%) of this MMT clay, determined by micro-X-ray fluorescence analysis (EDX spectrometer, Shimadzu, μEDX-1300), is: $SiO_2$ (62.2), $Al_2O_3$ (19.9), $Fe_2O_3$ (1.07), $TiO_2$ (0.15), MgO (6.77), CaO (1.13), $K_2O$ (1.10), $Na_2O$ (below detection limit) and others (7.68). Distilled acetone (Synth), glacial acetic acid (Synth) were used as-received.

### 2.2. Dispersion of clay in solvents

The clay particles were dispersed separately in a magnetic stirrer in each solvent used for this study: water, acetone and acetic acid. After 5 days in contact with these solvents, the clay dispersions were laid on the sample holder for XRD measurements. These clay dispersions were then dried under vacuum at 80 °C for 5 days and the resulting clay powders were also analyzed by XRD.

### 2.3. Preparation of CA/clay nanocomposites

Sodium montmorillonite dispersions, after 2 days immersion in the solvent, were added to the respective cellulose acetate solutions and mixed in a magnetic stirrer for two days at room temperature. The mixtures were prepared so as to give a final 95/5 CA/MMT weight ratio. Acetone (A) and acetic acid (AA) were used as pure solvents and mixtures of acetone/water (A/W) and acetic acid/water (AA/W) were also used for the preparation of cellulose acetate/clay nanocomposites. Films were prepared by solution casting on Teflon dishes and dried in an oven under air at different temperatures for 4 days. The experimental conditions for the preparation of pure cellulose acetate and nanocomposites are summarized in Table 1. In all cases, the cellulose acetate content was maintained at 11 wt% in the solution. The proportion of water used in mixtures with acetone and acetic acid was kept at 23 wt%. All the nanocomposites were prepared using 5% clay in relation to polymer.

### 2.4. Characterization

X-ray diffraction (XRD) measurements were performed using a Shimadzu XRD-7000 diffractometer in the reflection mode with an incident Cu $K_\alpha$ radiation ($\lambda = 0.1540$ nm) under 0.5°/min scan rate.

The X-ray microtomograph equipment consisted of a desktop X-ray micro-CT scanner (SkyScan 1074, Aartselaar, Belgium), equipped with a 768 × 576 pixel 8-bit X-ray camera in on-chip integration mode with the lens coupled to a scintillator (30 μm of resolution). As reference, a pure cellulose acetate film was layered over each nanocomposite film, prior to imaging.

The morphology of the cryogenically fractured samples was examined using a JEOL JSM-6340F field emission scanning electron microscope (FESEM), operating at an accelerating voltage of 3 kV.

The morphology and the elemental distribution in the nanocomposites were examined in a Carl Zeiss CEM 902 transmission electron microscope associated to electron loss spectroscopy, ESI-TEM. The microscope was operated at an acceleration voltage of 80 kV and equipped with a Castaing-Henry energy filter spectrometer within the column. Ultrathin sections, approximately 40 nm thick, were cut perpendicular to the film plane at −100 °C, in a Leica EM FC6 cryo-ultramicrotome. Elemental images were obtained for silicon (Si), the characteristic element in clay, using the three-window method. The energy-selecting slit was set at 132 eV for Si, with an energy slit width of 20 eV. The images were recorded using a Proscan high-speed slow-scan CCD camera and processed in the iTEM (Universal Imaging Platform) software.

**Table 1**
Experimental conditions for the preparation of pure cellulose acetate and cellulose acetate/montmorillonite nanocomposites by solution method.

| Composite code[a] | Solvent | CA/solvent (weight ratio) | Casting temperature (°C) |
|---|---|---|---|
| CA–A | Acetone | 11/89 | 50 |
| CA/MMT–A | Acetone | 11/89 | 50 |
| CA–A/W | Acetone/water | 11/66/23 | 50 |
| CA/MMT–A/W | Acetone/water | 11/66/23 | 50 |
| CA–AA | Acetic acid | 11/89 | 75 |
| CA/MMT–AA | Acetic acid | 11/89 | 75 |
| CA–AA/W | Acetic acid/water | 11/66/23 | 75 |
| CA/MMT–AA/W | Acetic acid/water | 11/66/23 | 75 |

[a] A = acetone; AA = acetic acid and W = water.

The dynamic mechanical analysis (DMA) was carried out in a Rheometric Scientific DMTA V Analyzer from −50 to 300 °C at 2 °C/min using a frequency of 1.0 Hz.

## 3. Results and discussion

### 3.1. Characterization of the clay with different solvents

Selection of an appropriate solvent plays a very important role in the preparation of nanocomposites by the solution intercalation method. The combination of high solubility of polymer and good dispersion of silicate layers is the primary criteria used in the selection of the solvent for efficient intercalation. Based on this, the effect of the solvent on the clay structure was investigated. To do so, clay particles were dispersed separately in each solvent used for this study: water, acetone and acetic acid. After swelling the clay particles in each solvent, a different behavior of the clay–solvent suspension stability was observed. While clay particles remained suspended in water, clay sedimentation in acetone and acetic acid was observed at the bottom of the recipient after a few minutes rest, as observed in Fig. 1. When water was used as the dispersion solvent, a more stable suspension was verified due to the higher swelling effect of water molecules in the silicate galleries.

Clay swelling in different solvents was also investigated by X-ray diffraction. The resulting X-ray diffraction patterns are presented in Fig. 2. The sodium montmorillonite pattern reveals a (001) reflection peak at around $2\theta = 7.3°$, corresponding to an interlayer spacing of 1.21 nm ($d_{001}$), while the patterns of the clay dispersed in water showed no peak. This result demonstrates that the water molecules can penetrate the interlayer space of the clay particles, reducing the attractive forces between the charged layer surfaces and the counterions, leading to layer separation and consequently to clay exfoliation. On the other hand, clay dispersed in acetone and acetic acid showed a shift of the reflection peak to lower angles ($2\theta = 5.3°$ and $2\theta = 5.5°$), corresponding to interlayer spacings of 1.67 and 1.60 nm, respectively. The swelling effect was thus less pronounced in acetone and acetic acid solvents, as previously observed (Fig. 1). The patterns of the corresponding clays after drying showed that the reflection peaks returned to nearly the initial angle values shown prior to the swelling test, suggesting reassembly of the layers to the initial stacked structure.

Understanding the interaction between clay particles and solvent is important to characterize nanocomposites formed by the solution intercalation method. The solubility parameter can be used to explain the clay structure in different solvents. Ho and Glinka [38] investigated the effect of Hansen's solubility parameters on the dispersion of organically modified clay in various solvents. It was found that the dispersion force of the solvent was the principal factor determining whether the organically modified clay layers remain suspended in the solvent, whereas the forces of polarity and hydrogen bond affect the tactoid formation of the clay in solution.

In this work, the results obtained from the dispersion of clay in the different solvents are consistent with the solubility parameters

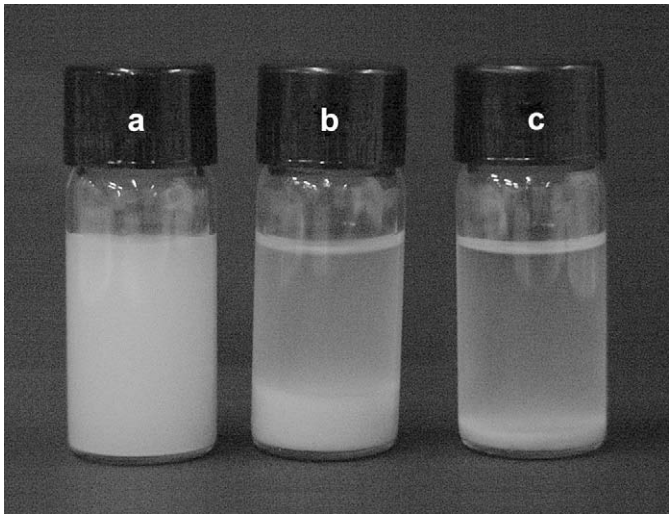


**Fig. 1.** Photographs of the suspension state of clay after 10 min rest in: (a) water, (b) acetone and (c) acetic acid.

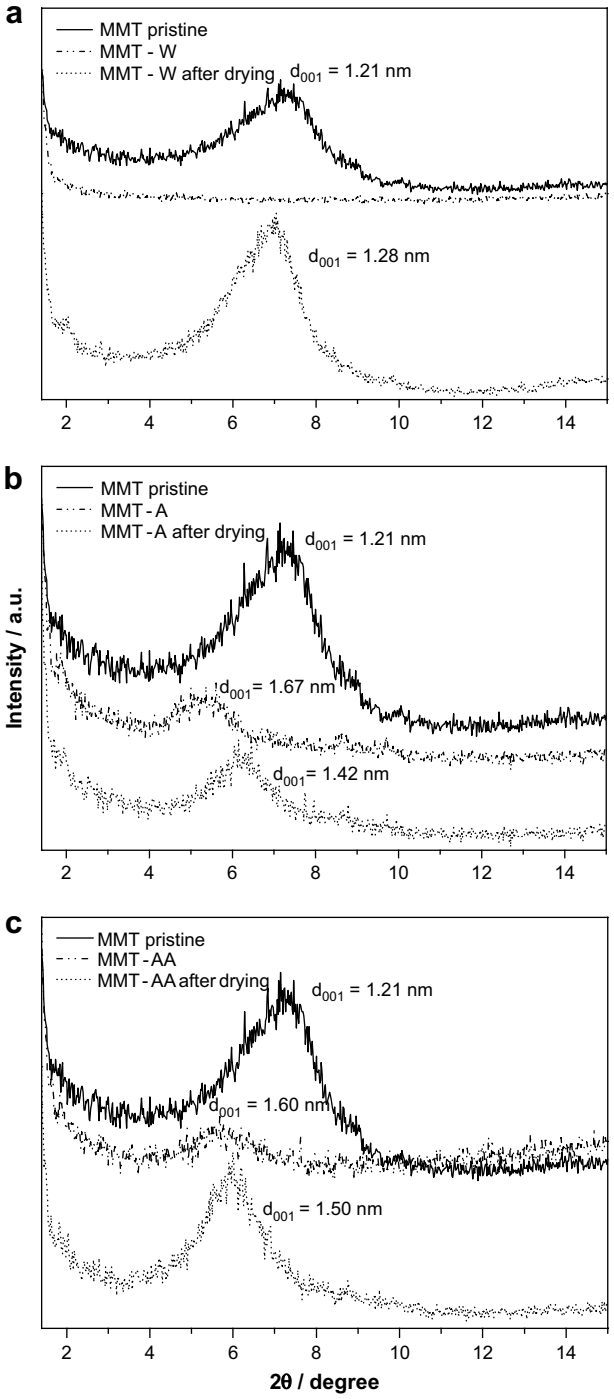


**Fig. 2.** XRD patterns for pristine clay (MMT), clay dispersed in solvent and clay after drying: (a) water, (b) acetone and (c) acetic acid.

of the solvents. The solubility parameter is described as a three component set: dispersive ($\delta_d$), permanent dipole–dipole or polar ($\delta_p$), and hydrogen bonding ($\delta_h$) interactions; where $\delta^2 = \delta_d^2 + \delta_p^2 + \delta_h^2$ [39]. Table 2 lists values of these terms for water, acetone and acetic acid.

Although it is not possible to obtain the solubility parameter of natural clay, it can be considered to be a highly polar material [40], due to the presence of negative superficial charges on the structure, that are counterbalanced by cations, generally $Na^+$ and $Ca^{2+}$. This polar character confers a high solubility parameter to the clay and permits the development of interactions with solvent of high solubility parameter, mainly through hydrogen bonding and ion–dipole interactions.

The higher values of $\delta_p$ and $\delta_h$ for water, compared to the corresponding values for acetone and acetic acid, can explain the exfoliation of the clay platelets in this solvent [40]. Comparing the swelling effect of acetone and acetic acid, it can be considered that there is no significant difference between these solvents, since the contribution of the polar and hydrogen bonding components of the solubility parameter counter balance each other. The intercalation and exfoliation of the clay platelets can be explained considering polar interactions with the structural oxygen of the clay layer as well as hydrogen bonding with the Si–OH groups from the layer edges. An additional contribution to the intercalation of acetic acid is the formation of complexes between the interlayer cations and the acetate ions.

Due to the better performance of water to delaminate the clay platelets, mixtures of acetone/water and acetic acid/water were also used as solvents in the preparation of CA/MMT nanocomposites.

### 3.2. Morphology of the CA/clay nanocomposites with different solvents

One advantage of polymer/clay nanocomposites is that the optical properties of the polymer are not significantly affected at lower clay contents. The thickness of individual clay layers is much smaller than the wavelength of visible light so that well exfoliated polymer/clay nanocomposites should be optically clear. Conventional clay microcomposites appear brown and opaque, while the nanocomposites keep good optical transparency. In this study, the cellulose acetate/clay films prepared from acetone, acetic acid and acetic acid/water solvents were transparent, which is evidence that the clay was dispersed in the polymer on a sub-micron scale. The distribution of clay particles was investigated by X-ray microtomographic analyses, where different cross-sections of the films were analyzed. Fig. 3 shows the tomographic images of the nanocomposites together with line profile plots as gray-level intensities measured along the stripes. The line profile analyses of the CA/MMT–A, CA/MMT–A/W and CA/MMT–AA nanocomposites showed a sharp peak at one side of the film and a gradual gray-level variation on the other side. These results indicate higher particle concentration in the lower film surface and depletion of clay particles in the upper surface, probably as a result of clay sedimentation during drying. In the case of films prepared from the acetone/water mixture, a reduction of the gray-level intensity across the film section is observed (Fig. 3(b)). This behavior is associated to the porous structure of the film due to the phase inversion mechanism occurring during film formation. For the nanocomposite prepared with acetic acid/water (CA/MMT–AA/W), the tomographic images showed a uniform gray-level intensity in the bulk, indicating nanocomposite homogeneity (Fig. 3(d)).

**Table 2**
Hansen solubility parameters for cellulose acetate and different solvents studied in the CA/MMT nanocomposites system at 25 °C [39].

| Sample | Solubility parameters $(MPa)^{1/2}$ | | | |
|---|---|---|---|---|
| | $\delta$ | $\delta_d$ | $\delta_p$ | $\delta_h$ |
| *Polymer* | | | | |
| Cellulose acetate | 25.1 | 18.6 | 12.7 | 11.0 |
| *Solvent* | | | | |
| Acetone | 20.1 | 15.5 | 10.4 | 7.0 |
| Acetic acid | 21.3 | 14.5 | 8.0 | 13.5 |
| Water | 47.9 | 15.5 | 16.0 | 42.4 |

The morphological characteristics of pure CA and nanocomposite bulk fractures were investigated by FESEM and some micrographs are presented in Fig. 4. The morphology of the fractured surface of pure cellulose acetate reveals a smooth fracture surface and indicates a dense polymer film (Fig. 4(a)). The micrographs of CA/MMT–A and CA/MMT–AA nanocomposites show the same fracture characteristics, although some clay particles wrapped up can also be observed in the polymeric matrix. The inset in Fig. 4(b) shows one clay particle inside the CA matrix, which indicates good adhesion at the clay–polymer interface. On the other hand, the micrographs of the nanocomposites prepared with solvent/water mixtures, i.e. CA/MMT–A/W and CA/MMT–AA/W nanocomposites, showed a rougher fracture surface and the absence of larger tactoids (Fig. 4(c) and (e)). Due to the presence of water in the solvent mixtures, film formation follows the phase inversion process by which the polymer solution evolves into a swollen three-dimensional macromolecular network or gel.

Phase separation via phase inversion processes has been extensively studied for the CA/acetone/water system as a model system to investigate polymeric membrane formation [41–44]. The solid–liquid phase separation can take place during the casting process since water was present in the solvent mixtures. When acetone–water was used as the solvent mixture, this phase separation was promoted by the relatively rapid evaporation of the good and more volatile solvent (acetone), which caused an increase in the concentration of the less volatile nonsolvent (water) in the mixture [45]. Ultimately, this process can create a pore structure in the film, as observed in the tomographic image presented in Fig. 3(b). On the other hand, when the acetic acid/water mixture was used as a casting solvent, the higher volatility of water led to phase separation promoted by the increase in polymer concentration during solvent evaporation. In this case, a more dense film was obtained when compared with the film prepared from the acetone–water mixture.

The interlayer distances ($d_{001}$) of the basal reflection peaks of natural MMT and the CA/MMT nanocomposite were determined from X-ray diffraction. These results are shown in Table 3. Based on prior results from the X-ray microtomograph, great attention was given to the differences between the surfaces of the films, i.e. the upper face, formed in contact with air, and the lower face, formed in contact with the mold surface. The sodium montmorillonite pattern revealed an interlayer spacing of 1.21 nm ($d_{001}$). The patterns of CA/MMT prepared with acetone showed that this reflection peak shifted to lower angles, corresponding to an interlayer spacing of 1.44 nm for the two faces. The same peak was not detected for upper faces of the CA/MMT–A/W, CA/MMT–AA and CA/MMT–AA/W nanocomposites, probably due to the lower concentrations of the clay particles in this face of the films. On the other hand, the XRD pattern of the lower faces of the CA/MMT–A/W, CA/MMT–AA and CA/MMT–AA/W nanocomposites showed that the (001) reflection peak shifted to 1.42, 1.40 and 1.60 nm, respectively. These results indicated that no significant increase in the interlayer spacing was verified, suggesting that the CA polymer was not able to intercalate into the clay gallery.

XRD is an extremely valuable technique, however, the results can be ambiguous and cannot be interpreted unless supporting evidence is offered, generally through representative microscopic images. Therefore, the structure of the silicate platelets was also

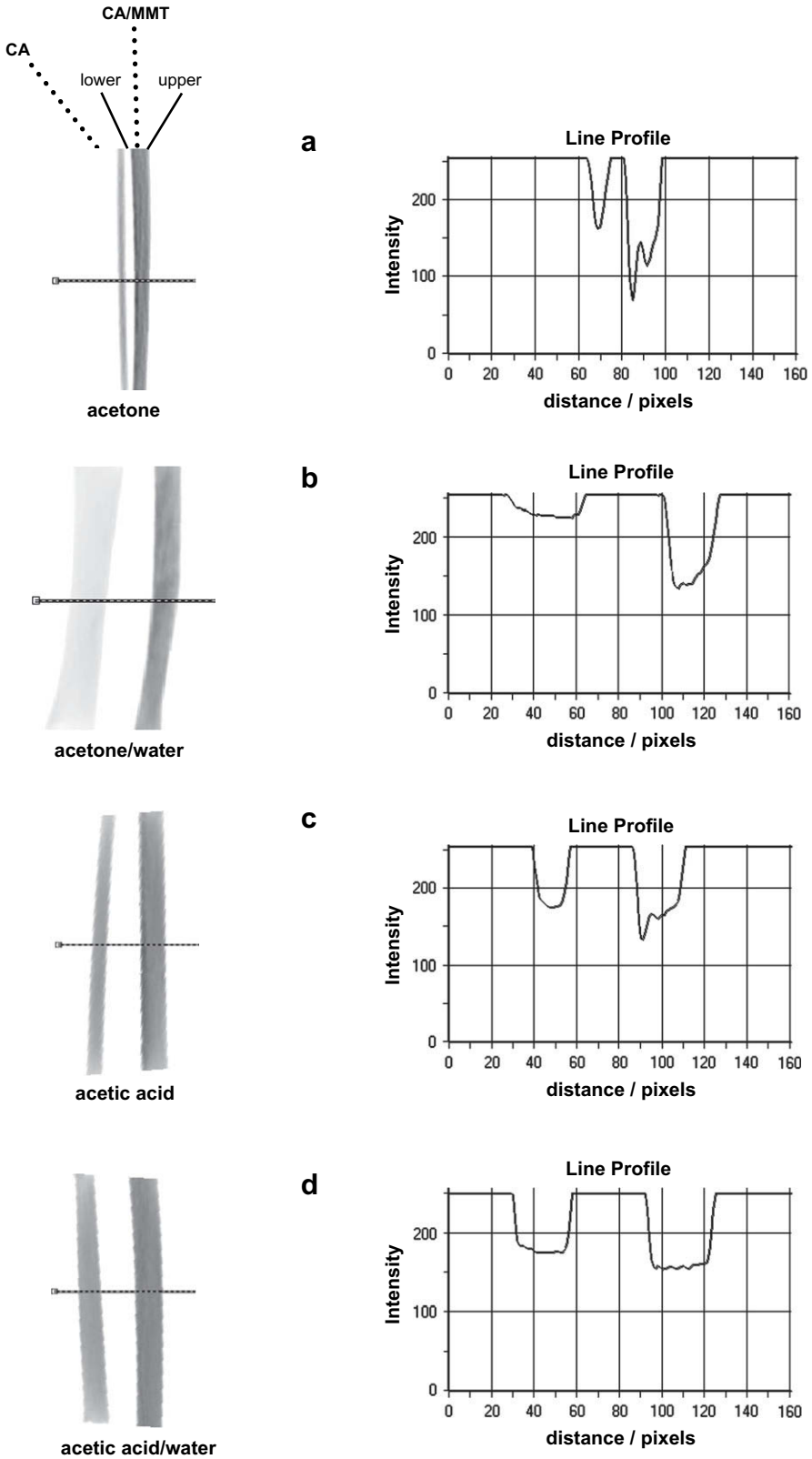


**Fig. 3.** X-ray microtomographic images: (a) CA/MMT–A, (b) CA/MMT–A/W, (c) CA/MMT–AA and (d) CA/MMT–AA/W nanocomposites.

investigated by TEM to evaluate the morphological behavior of the polymer–clay systems prepared through the solution intercalation method. The electron micrographs of the bulk thin sections of CA/MMT–A and CA/MMT–AA nanocomposites (Fig. 5(a) and (c), respectively) showed mainly tactoids swollen by the polymer. The micrograph of the CA/MMT–A/W nanocomposite (Fig. 5(b)) showed the presence of swollen tactoids as well as microvoids characteristic of the porous morphology of this material. However, the CA/MMT–AA/W nanocomposite consisted predominantly of exfoliated silicate platelets and a small number of layered stacks

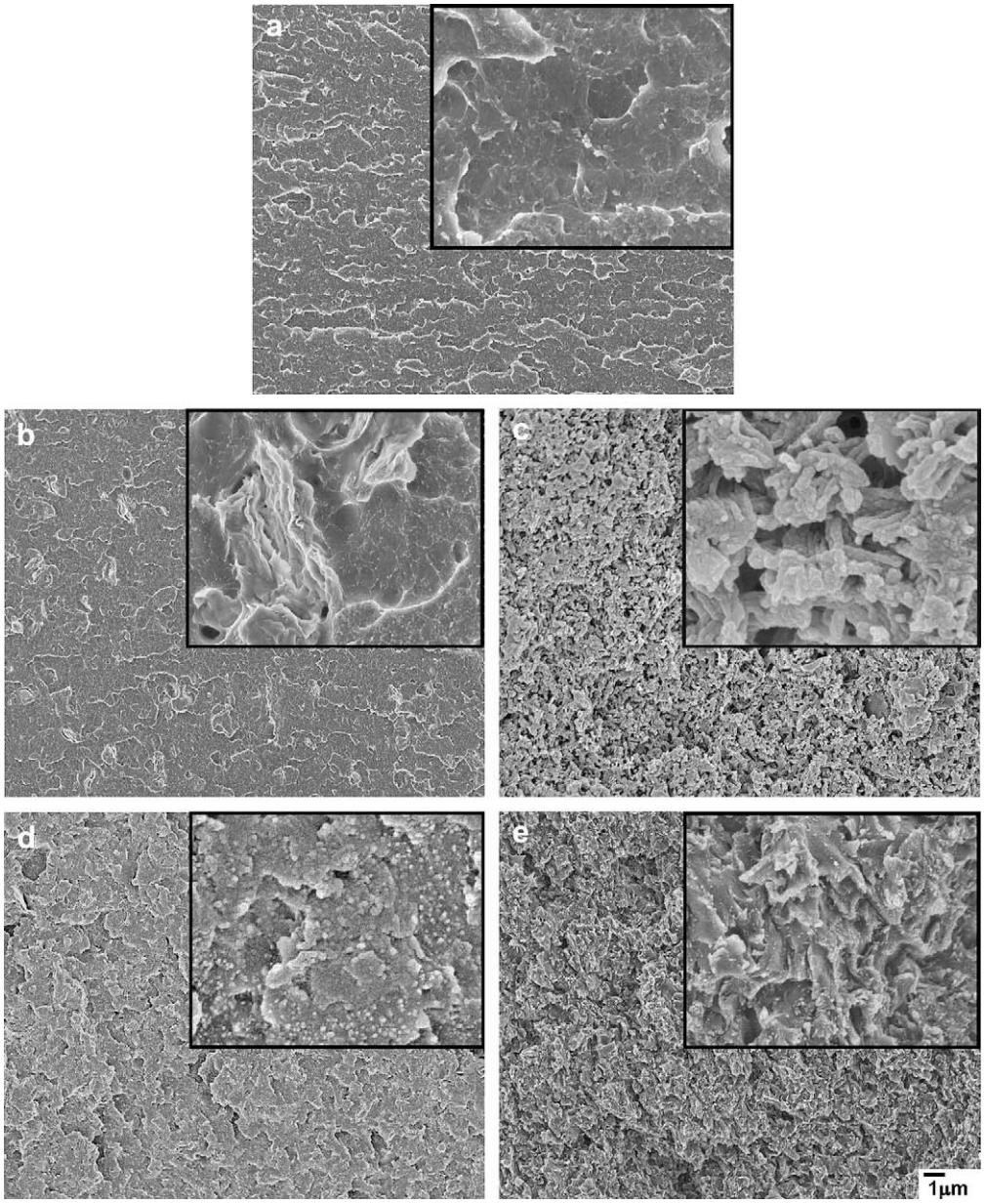


**Fig. 4.** FESEM micrographs of bulk fractures: (a) CA–A, (b) CA/MMT–A, (c) CA/MMT–A/W, (d) CA/MMT–AA and (e) CA/MMT–AA/W nanocomposites. Inset: magnified views.

(Fig. 5(d)). It is noteworthy that the presence of exfoliated platelets was not always easily detected in TEM observations, due to the lower contrast of individual clay layers in the polymeric matrix. Because of this the thin bulk sections were also examined by ESI-TEM, through the mapping of the silicon distribution. In Fig. 6, the bright field image is shown side by side with the silicon mapping image for the CA/MMT–AA/W nanocomposite. In the bright field image (Fig. 6(a)), the dark regions are related to the denser phase, i.e. the silicate platelets, and correspond to the white regions in the silicon mapping (Fig. 6(b)). So, the silicon mapping clearly shows the clay platelet arrangements in the cellulose acetate film. A roughly regularly spaced and relatively curved array of layers, showing interlayer distances of approximately $43 \pm 8$ nm for the CA/MMT–AA/W nanocomposites, can be seen. In the literature, distances greater than 22 nm are associated to exfoliated structures since the electrostatic and van der Waals forces are reduced at higher clay layer separation distances [46]. In the present work, the nearly spaced layers can be assigned to a uniform distribution of CA molecules in between the silicate layers [47–50]. The TEM images also show that the polymer and clay domains are well connected, evidenced by the integrity of the clay–polymer interfaces.

Based on XRD results and TEM observations, a schematic representation of the morphologies of CA/MMT nanocomposites in different solvents is proposed, as can be seen from Fig. 7.

**Table 3**
Interlayer distance of clay and nanocomposites prepared with different solvents.

| Samples | $d_{001}$ (nm) upper[a] | $d_{001}$ (nm) lower[b] |
|---|---|---|
| Pristine MMT | 1.21 | 1.21 |
| CA/MMT–A | 1.44 | 1.44 |
| CA/MMT–A/W | No peak | 1.42 |
| CA/MMT–AA | No peak | 1.40 |
| CA/MMT–AA/W | No peak | 1.60 |

[a] Upper = dried in contact with air.
[b] Lower = dried in contact with the plastic mold surface.

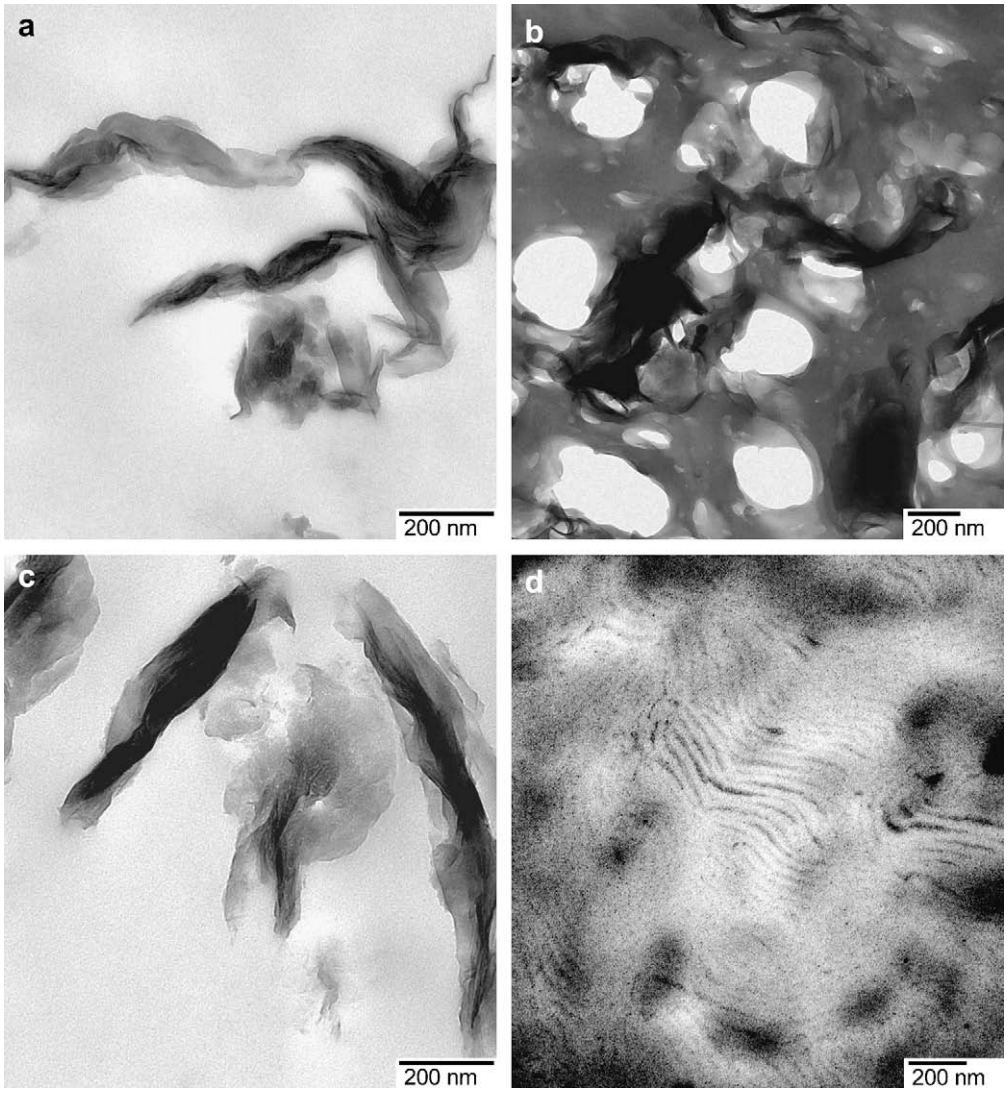


**Fig. 5.** TEM images of (a) CA/MMT–A, (b) CA/MMT–A/W, (c) CA/MMT–AA and (d) CA/MMT–AA/W nanocomposites.

### 3.3. Dynamical mechanical properties of the CA/clay nanocomposites

Fig. 8 shows the temperature dependence of the storage modulus ($E'$) and tan $\delta$ for the pure CA and the CA/MMT nanocomposites prepared from different solvents. Table 4 presents the corresponding values for the storage modulus at two temperatures, 25 °C and 100 °C, and the glass transition temperatures ($T_g$). The tan $\delta$ curves of the pure CA prepared with acetone showed a peak at 161 °C corresponding to the glass transition temperature. A notable increase in the value of the $T_g$ was verified for the other CA films, where the observed values for films prepared from acetic acid, acetone–water and acetic acid–water solvents were 211 °C, 221 °C and 221 °C, respectively.

The solubility of CA in solvents depends on a number of factors including the degree of substitution (DS) of the acetyl groups as well as the distribution of substituents along the polymer chain. Cellulose acetate with a DS greater than 1 tends to be insoluble in aqueous solutions but soluble in many organic solvent systems.

The CA behavior in solvents that selectively interact with specific functional groups on the polymer chain may provide some insights into the film properties. Acetone and acetic acid are considered good solvents for the CA polymer [41,51–53], as indicated by the proximity of the solubility parameter values (Table 2), whereas pure water is a nonsolvent. In the case of the CA–acetone solution, the carbonyl groups present in acetone interact with acetyl groups of CA chains and, to a lesser extent, with hydroxyl groups. In the case of the CA–acetic acid solution, the carboxyl groups on acetic acid interact with acetyl and hydroxyl groups on the CA molecule. The addition of a nonsolvent (i.e. water) to CA–acetone or CA–acetic acid solutions weakens these interactive bonds and shifts some acetone or acetic acid molecules to interact with water. The bond breaking leads to intra- and intermolecular interactions between unbonded or "free" CA chains and to the formation of CA associates. Thus, CA molecules may experience intra- and intermolecular interactions, particularly hydrogen bonding, with the presence of water in solution. These hydrogen bondings bridge neighbouring cellulose structural units' segments, thus making CA molecules particularly rigid. The strength and amount of such interactions are responsible for complex molecular associations of CA molecules [47–50]. In the present case, the variations in chain rigidity are expressed in terms of $T_g$ values of CA films prepared from different solvents.

The nanocomposites prepared with acetone showed a slight increase in the storage modulus ($E'$) in relation to the pure CA film prepared with the same solvent. The tan $\delta$ curves showed two

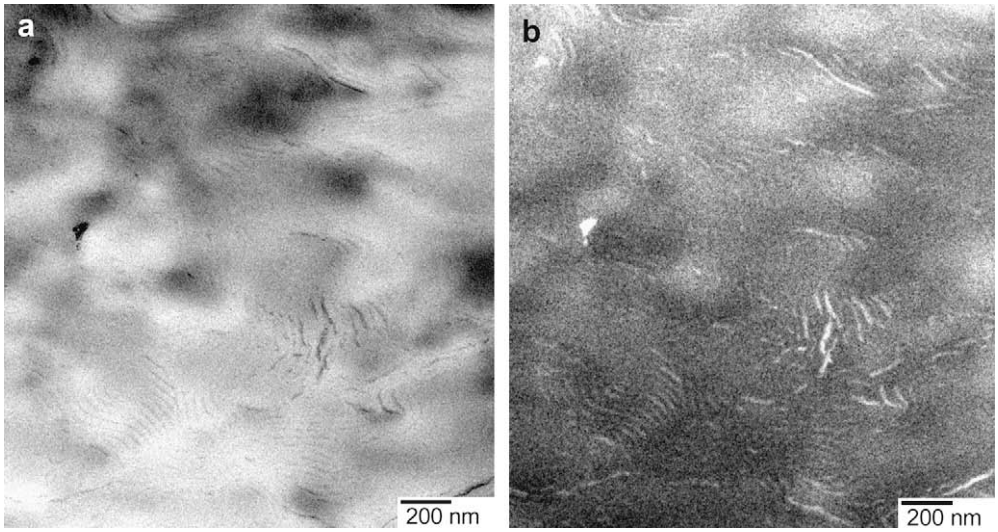


**Fig. 6.** ESI-TEM images of the CA/MMT–AA/W nanocomposite: (a) bright field and (b) silicon map.

peaks, the first at 160 °C corresponding to a secondary transition, and a second peak at 202 °C corresponding to the glass transition temperature. The tan $\delta$ curves of the nanocomposites prepared with acetone/water (CA/MMT–A/W) presented a peak at 220 °C corresponding to the $T_g$ and the $E'$ curve showed a modulus that increased by approximately 150% in relation to the pure CA film prepared with the same solvent. On the other hand, comparing the values of the storage modulus of CA/MMT–A/W and CA/MMT–A films, as well as CA–A/W and CA–A, the lower value obtained for the formers is due to their porous morphology. For the CA/MMT–AA

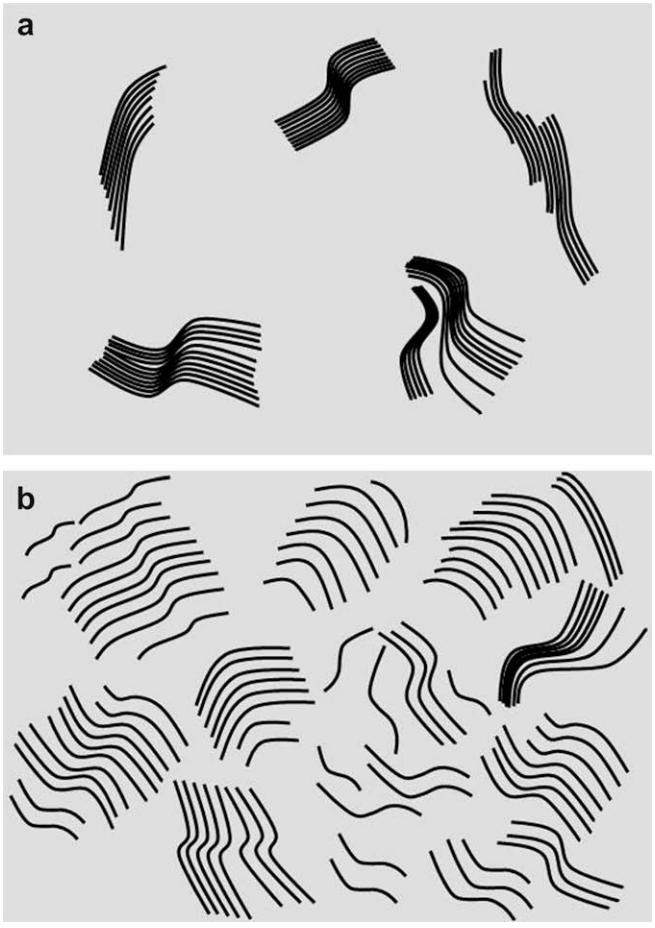


**Fig. 7.** Schematic representation of the morphologies of CA/MMT nanocomposites prepared by the solution method: (a) clay tactoids swollen by the polymer and (b) exfoliated silicate platelets dispersed in the polymeric matrix.

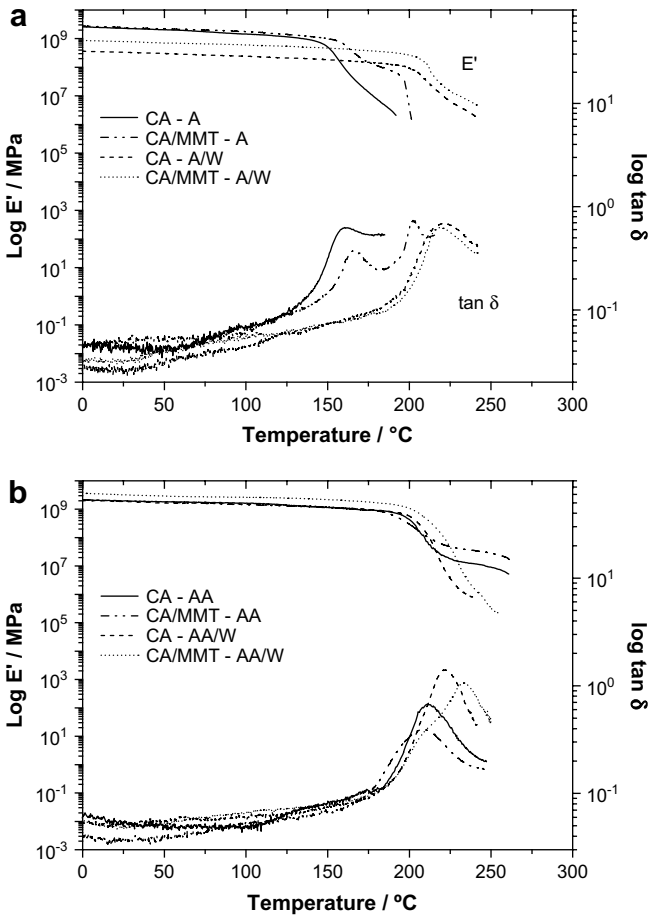


**Fig. 8.** DMA curves of the storage modulus ($E'$) and tan $\delta$ for: (a) pure CA and CA/MMT nanocomposites prepared with acetone and acetone/water and (b) pure CA and CA/MMT nanocomposites prepared with acetic acid and acetic acid/water.

**Table 4**
Glass transition temperature ($T_g$) and storage modulus ($E'$) of pure CA and CA/MMT nanocomposites prepared with different solvents.

| Sample | $T_g$ (°C) | $E'$ (MPa)[a] | $E'$ (MPa)[b] |
|---|---|---|---|
| CA–A | 161 | 2200 | 1450 |
| CA/MMT–A | 202 | 2400 | 1750 |
| CA–A/W | 221 | 330 | 240 |
| CA/MMT–A/W | 219 | 800 | 610 |
| CA–AA | 211 | 2000 | 1600 |
| CA/MMT–AA | 208 | 2000 | 1600 |
| CA–AA/W | 221 | 1900 | 1500 |
| CA/MMT–AA/W | 233 | 3300 | 2700 |

[a] Storage modulus measured at 25 °C.
[b] Storage modulus measured at 100 °C.

nanocomposite no significant variation in $T_g$ was observed, whereas for the CA/MMT–AA/W nanocomposite a higher glass transition temperature was detected as compared to the respective film without clay. The storage modulus for the CA/MMT–AA nanocomposite was invariant at temperatures below 200 °C but the modulus for the CA/MMT–AA/W nanocomposite showed a significant increase over the whole range of temperatures.

The storage modulus can be used to evaluate the reinforcement effect of the high modulus phase dispersed in the polymeric matrix. Thus, its enhancement is assigned to the presence of clay particles and the interfacial strength [54]. On the other hand, the increase of glass transition temperature is attributed to the restriction of the segmental motion of the polymer backbone and can indicate favorable interactions between the polymer and the silicate layers. Moreover, special arrangements of the dispersed layers can help to establish edge-to-edge and edge-to-face interactions between them, resulting in a percolation structure. Krishnamoorti et al. [55] proposed a model that explains the formation of this three-dimensional network. In this model, the structure of the nanocomposites is made up of stacks of individual layers and tactoids, which present a considerable anisotropy and form a three-dimensional network, whose percolation hinders the complete rotation and relaxation of these particles. The model, involving clay tactoids and individual layers that interact with polymer molecules, would therefore be responsible for the restriction of polymer chain mobility.

In the present work, the observed differences in the dynamical mechanical behavior of the CA nanocomposites are mainly ascribed to the polymer–clay interactions and the specific morphological characteristics of each nanocomposite. Considering that CA is a high-$T_g$ polymer these differences are notable, especially for nanocomposites showing exfoliated morphology, as is the case of the CA/MMT nanocomposite prepared from the acetic acid/water solvent mixture. In this case, the glass transition temperature and storage modulus increased from 221 °C to 233 °C and from 1900 MPa to 3300 MPa, respectively.

Since the prominent properties of polymer–clay nanocomposites are observed when delamination or intercalation is achieved, much research has been conducted to predict the clay morphology in a polymer matrix. Jang et al. [40] recently observed a close relationship between the polymer solubility parameter and clay morphology. Using a natural clay, the delaminated morphology was only achieved when combined with a polymer having a high solubility parameter, such as poly(acrylonitrile) (26.1 $MPa^{1/2}$), and using an *in situ* polymerization method. The results obtained in the present work confirm that polymers with high solubility parameters, such as cellulose acetate (25.1 $MPa^{1/2}$, Table 2), present favorable interactions with sodium clay. However, the clay–solvent interaction has a major effect on the clay morphology and, consequently, on the nanocomposite properties. To understand the results, it is necessary to understand the mechanism of nanocomposite formation in solution. When the solvent used is able to effectively swell the clay gallery, the clay interlayer spacing is sufficiently expanded and CA chains or associates in solution can be accommodated in the gallery opening. In this case, the highly polar character of the solvent together with the ability of H-bonding between solvent and silicate platelets could overcome the strong electrostatic interaction between the clay layers and promote the required expansion. In dried nanocomposites, the confined polymer chains interact with the clay surface through polar and hydrogen bonds, which are responsible for clay–polymer interfacial adhesion.

## 4. Conclusions

Two important factors were verified as being influential to control the morphology and properties of cellulose acetate/natural clay nanocomposites prepared by solution method. First, a proper selection of solvent is desirable to promote favorable clay–solvent interactions and, consequently, the expansion of the clay gallery. This is initially required to enable the entry of the polymer chain between the clay layers so that platelet exfoliation can occur during casting process. The second influential factor is the chemical affinity, e.g. thermodynamic interactions, between the polymer molecules and silicate surface.

The results described in this paper verify that the swelling of clay by the polymer solution was more effective in the presence of water, especially in the mixture with acetic acid. This effect is attributed to specific polar interactions, H-bonds and complex formation between cellulose acetate chains and solvent molecules. Another important aspect is the chemical affinity between polymer chain and clay surface, which was indicated by some of results obtained. Thus, the solvent effect together with clay–polymer interactions plays an important role in the control of the nanocomposites morphology and properties.

## Acknowledgements

CNPq and FAPESP are acknowledged for financial support. R.B.R. thanks CAPES for a fellowship.

## References

[1] LeBaron PC, Wang Z, Pinnavaia TJ. Appl Clay Sci 1999;15:11–29.
[2] Ray SS, Yamada K, Okamato M, Ueda K. Polymer 2003;44:857–66.
[3] Fornes TD, Yoon PJ, Hunter DL, Keskkula H, Paul DR. Polymer 2002;43:5915–33.
[4] Fornes TD, Paul DR. Polymer 2003;44:3945–61.
[5] Alexandre M, Dubois P. Mater Sci Eng 2000;28:1–63.
[6] Ruiz-Hitzky E, Darder M, Aranda P. J Mater Chem 2005;15:3650–62.
[7] Wang XY, Du YM, Luo JW. Carbohydr Polym 2007;69:41–9.
[8] Zhuang H, Zheng JP, Gao H. J Mater Sci Mater Med 2007;18:951–7.
[9] Shih YF, Wang TY, Jeng RJ. J Polym Environ 2007;15:151–8.
[10] Ray SS, Okamoto M. Prog Polym Sci 2003;28:1539–641.
[11] Ray SS, Bousmina M. Prog Mater Sci 2005;50:962–1079.
[12] Fomin VA, Guzeev VV. Prog Rubber Plast Technol 2001;17:186–204.
[13] Wibowo AC, Misra M, Park HM, Drzal LT, Schlek R, Mohanty AK. Compos Part A Appl Sci Manuf 2006;37:1428–33.
[14] Mohanty AK, Misra M, Park HM, Drzal LT, Wibowo AC. US2005 051054-A1; Wo 2005 5026429-A2; US 6893492-B2.
[15] Ray SS, Okamoto K, Yamada K, Okamoto M. Nano Lett 2002;2:423–6.
[16] Paul MA, Alexandre M, Degee P, Henrist C, Rulmont A, Dubois P. Polymer 2003;44:443–50.
[17] Maiti P, Batt CA, Giannelis EP. Polym Mater Sci Eng 2003;88:58–69.
[18] Chen GX, Hao GJ, Guo TY, Song MD, Zhang BH. J Appl Polym Sci 2004;93:655–61.
[19] Park HM, Li X, Jin CZ, Park CY, Cho WJ, Ha CK. Macromol Mater Eng 2002;287:553–8.
[20] Park HM, Lee WK, Park CY, Cho WJ, Ha CS. J Mater Sci 2003;38:909–15.
[21] Uyama H, Kuwabara M, Tsujimoto T, Nakano M, Usuki A, Kobayashi S. Chem Mater 2003;15:2492–504.
[22] Miyagawa H, Misra M, Drzal LT, Mohanty AK. Polymer 2005;46:445–53.
[23] Park HM, Liang X, Mohanty AK, Misra M, Drzal LT. Macromolecules 2004;37:9076–82.
[24] White LA. J Appl Polym Sci 2004;92:2125–31.

[25] Park HM, Mohanty AK, Drzal LT, Lee E, Mielewski DF, Misra M. J Polym Environ 2006;14:27–35.
[26] Zheng JP, Ping Li, Ma YL, Yao KD. J Appl Polym Sci 2002;86:1189–94.
[27] Watzke HJ, Dieschbourg C. Adv Colloid Interface Sci 1994;50:1–14.
[28] Darder M, Colilla M, Ruiz-Hitzky E. Chem Mater 2003;15:3774–80.
[29] Darder M, Colilla M, Ruiz-Hitzky E. Appl Clay Sci 2005;25:199–208.
[30] Di Y, Iannace S, E Di Maio, Nicolais L. J Polym Sci Part B Polym Phys 2005;43:689–98.
[31] Mohanty AK, Wibowo A, Misra M, Drzal LT. Polym Eng Sci 2003;43:1151–61.
[32] Kim J, Yun S. Macromolecules 2006;39:4202–6.
[33] Balser K, Eicher T, Wnadel M, Astheinmer HJ. In: Gerhartz W, Yamamoto YS, editors. Cellulose esters. Ulmann's encyclopedia of industrial chemistry, vol. A5. VCH; 1986. p. 438–57.
[34] Edgar KJ, Buchanan CM, Debenham JS, Rundquist PA, Seiler BD, Shelton MC, et al. Prog Polym Sci 2001;26:1605–88.
[35] Park HM, Misra M, Drzal LT, Mohanty AK. Biomacromolecules 2004;5:2281–8.
[36] Li Y, Ishida H. Polymer 2003;44:6571–7.
[37] Shen Z, Simon GP, Cheng YB. Polymer 2002;43:4251–60.
[38] Ho DL, Glinka CJ. Chem Mater 2003;15:1309–12.
[39] Grulke EA. In: Brandrup J, Immergut EH, editors. Solubility parameter values. Polymer handbook. 3rd ed., vol. II. New York: Jonh Wiley & Sons Inc.; 1989. p. 519–59.
[40] Jang BN, Wang D, Wilkie CA. Macromolecules 2005;38:6533–43.
[41] Shojaie SS, Krantz WB, Greenberg AR. J Mater Process Manuf Sci 1992;1: 181–94.
[42] Greenberg AR, Shojaie SS, Krantz WB, Tantekin-Ersolmaz B. J Membr Sci 1995;107:249–61.
[43] Altinkaya AS, Ozbas B. J Membr Sci 2004;230:71–89.
[44] Lee H, Chaudhuri SR, Krantz WB, Hwang ST. J Membr Sci 2006;284:161–72.
[45] Flory PJ. Principles of polymer chemistry. Ithaca: Cornell University Press; 1953.
[46] Koo CM, Ouk KS, Jae C. Macromolecules 2003;36:2748–57.
[47] Schulz L, Seger B, Burchard W. Macromol Chem Phys 2000;201:2008–22.
[48] Appaw C, Gilbert RD, Khan SA. Biomacromolecules 2007;8:1541–7.
[49] Kawanishi H, Tsunashima Y, Okada S, Horii F. J Chem Phys 1998;108:6014–25.
[50] Kawanishi H, Tsunashima Y, Okada S, Horii F. Macromolecules 2000;33: 2092–7.
[51] Fuchs O. In: Brandrup J, Immergut EH, editors. Solvents and non-solvents for polymers. Polymer handbook. 3rd ed., vol. II. New York: Jonh Wiley & Sons Inc.; 1989. p. 400.
[52] Liu H, Hsieh Y. J Polym Sci Part B Polym Phys 2002;40:2119–29.
[53] Han SO, Youk JH, Min KD, Kang YO, Park WH. Mater Lett 2008;62:759–62.
[54] Rao YQ, Pochan JM. Macromolecules 2007;40:290–6.
[55] Krishnamoorti R, Ren J, Silva AS. Macromolecules 2000;33:3739–46.